Supporting Material

Singlet oxygen-mediated water purification by Cu^0 anchored amorphous FeOOH via oxygen activation

Yuwei Yang[1], Dong Li[1], Xiaoyu Zheng[1], Xuguang Li (✉)[1], Haiqiang Qi[1], Wen Song[1], Yunhui Zhang[2], Liangguo Yan[1]

1 School of Water Conservancy and Environment, University of Jinan, Jinan 250022, China

2 College of Environmental Science and Engineering, Tongji University, Shanghai 200092, China

This Supporting Information provides:

Total number of pages: 52

Total number of Text: 11

Total number of Figures: 18

Total number of Tables: 10

✉ Corresponding author
E-mail: stu_lixg@ujn.edu.cn

Cu^0/PMS system).

Table S10 Impact assessment for the treatment of 1 ton OTC wastewater (a-FeOOH-Cu^0/air system).

Fig. S1 (a) Preparation process of the a-FeOOH-Cu^0 catalyst, and XRD patterns of (b) Cu0, α-FeOOH, α-FeOOH-Cu^0 and (c) Cu^0, β-FeOOH, β-FeOOH-Cu^0.

Fig. S2 SEM images of (a, c) a-FeOOH and (b, d) a-FeOOH-Cu^0.

Fig. S3 N_2 adsorption-desorption isotherms of (c) a-FeOOH-Cu^0 and (d) a-FeOOH; (c) EIS of Cu^0, a-FeOOH-Cu^0 and a-FeOOH.

Fig. S4 Normalized Cu (a) valence state variation and (b) wavelet transform of a-FeOOH-Cu^0, Cu_2O, Cu-foil, CuO and CuPc. Normalized Fe (c) valence state variation and (d) wavelet transform of a-FeOOH-Cu^0, Fe_2O_3, Fe-foil, Fe_3O_4, FeO, and FePc.

Fig. S5 (a) The effect of physically mixing a-FeOOH and Cu^0 on the degradation efficiency; (b) the degradation process of OTC by a-FeOOH-Cu^0, measured and comparatively analyzed using ultraviolet spectroscopy (UV) and high-performance liquid chromatography (HPLC).

Fig. S6 The degradation effects of different catalysts at (a) pH=5, (b) pH=7, (c) pH=8, (d) OTC = 5 mg/L, (e) OTC = 10 mg/L, and (f) OTC = 20 mg/L.

Fig. S7 (a) The degradation of OTC itself under different pH conditions; (b) the variation of pH during the reaction process; (c) fitting curves of the initial concentration (C_0) versus initial reaction rate (r_0) for OTC with different catalysts; and (d) OTC degradation efficiency by a-FeOOH-Cu^0 under N_2 and O_2 atmospheres.

Fig. S8 OTC degradation efficiency at (a) different catalyst concentrations and (b) aeration rates; (c) variation of dissolved oxygen in different systems during the reaction.

Fig. S9 The effects of different concentrations of (a) Cl^-, (b) NO_3^-, (c) HCO_3^-, (d) SO_4^{2-}, and (e) HA on the degradation of OTC; and (f) degradation effects of OTC in different actual water bodies.

Fig. S10 (a) XPS and (b) XRD spectra of a-FeOOH-Cu^0 before and after the reaction; (c) degradation of OTC by leached ions and a-FeOOH-Cu^0; and (d) degradation of different organic compounds by a-FeOOH-Cu^0.

Fig. S11 (a) HPLC data showing •OH changes during the reaction processes of Cu^0 and a-FeOOH-Cu^0; spectral data showing $^{\bullet}O_2^-$ changes during the (b) Cu^0 and (c) a-FeOOH-Cu^0 reaction processes; and (d) HPLC data showing $^1O_2$ changes during the reaction processes of Cu^0 and a-FeOOH-Cu^0.

Fig. S12 (a, b) Spectral data on changes in H_2O_2 content during the reaction processes of Cu^0 and a-FeOOH-Cu^0; (c) Linear fitting spectra of H_2O_2 concentration versus absorption intensity; (d) Transient concentration of H_2O_2 in different reaction systems.

Fig. S13 Quenching experiments for the degradation of OTC by (a) Cu^0 and (b) a-FeOOH-Cu^0 with TBA, CAT, TEMP, and p-BQ, respectively; (c) the effect of different concentrations of TBA, CAT, TEMP, and p-BQ on OTC degradation efficiency; (d) the effect of high-valent metals on the catalytic degradation performance in different systems; (e) detection of high-valent copper; and (f) contribution ratios of reactive oxygen species (ROS).

Fig. S14 Spectral data on changes in $^1O_2$ content during the Cu^0 and a-FeOOH-Cu^0 reaction processes in both the absence (a, b) and presence of p-BQ (c, d).

Fig. S15 (a) Changes in the O valence state composition and (b) O 1s XPS spectra of a-FeOOH-Cu^0 before and after the reaction.

Fig. S16 (a) The degradation pathway of OTC and (b) UPLC-MS analysis of its intermediates in the reaction with a-FeOOH-Cu^0.

Fig. S17 The preparation of a-FeOOH-Cu^0 aerogel.

Fig. S18 Energy-dispersive X-ray elemental mapping of a-FeOOH-Cu^0 aerogel.

Text S1 Chemicals.

Goethite (α-FeOOH), Akaganeite (β-FeOOH), Ferrous sulfate ($FeSO_4·7H_2O$), Sodium borohydride ($NaBH_4$), anhydrous copper sulfate ($CuSO_4$), ferric nitrate ($Fe(NO_3)_3·9H_2O$), ammonium bicarbonate (NH_4HCO_3), Sulfamethoxazole (SMX), Ciprofloxacin (CIP), Bisphenol A (BPA), oxytetracycline (OTC), tetracycline (TC), methylphenyl sulfoxide (PMSO), norfloxacin (NFX), p-benzoquinone (PBQ), catalase (CAT), potassium bromate ($KBrO_3$), Nitrotetrazolium blue chloride (NBT), furfuryl alcohol (FFA), benzoic acid (BA), potassium hydrogen phthalate ($C_8H_5KO_4$) , Anhydrous ethanol and potassium iodide (KI)were purchased from McLean Company, Shanghai, China.

Methylene blue (MB) and hydrochloric acid (HCl) were purchased from Tianjin Damao Company, China.

Rhodamine B (RhB), dimethyl sulfoxide (DMSO), tert-butanol (TBA) were purchased from Tianjin Fuyu Company, China.

9,10-Diphenyl onion (DPA) was purchased from Shanghai Amec Biochemical Company, China.

Sodium hydroxide (NaOH) was purchased from Sinopharm Group Corporation, China.

The purity of all the above reagents is analytical grade.

Text S2 Analytical methods.

The structures of samples were performed by X-ray diffractometer (XRD, Rigaku, SmartLab SE) with Cu Ka source irradiation. Fourier transform infrared (FT-IR) spectra were recorded on a NicoletiS50 FT-IR spectrometer (Thermo Fisher, Nicolet iS50) in a range of 400-4000 cm^{-1}. The surface morphologies and inner structures of the samples were analyzed by scanning electron microscopy (SEM, Japan, Regulus8220), electronic differential system (EDS, XFlash 6160), transmission electron microscopy (TEM), and high-resolution TEM (HRTEM, jem2100, Japan). Using a Micromeritics ASAP 2020M system, the surface areas of the samples' Brunauer-Emmett-Teller (BET) were calculated. The N_2 adsorption / desorption experiment was carried out by a BELSORP MaxII (Japan) to examine the surface area and pore dispersion of the catalyst.

The produced radicals were determined by a Bruker A300 electron paramagnetic resonance (EPR) spectrometer using DMPO (5,5- dimethyl-1-pyrroline-N-oxide) and TEMP (4-hydroxy-2,2,6,6-tetramethylpiperidinyl-oxy) as a probe. On an electrochemical workstation (CHI-760E, China) using a traditional three-electrode system in a 0.1 mol/L Na_2SO_4 electrolyte, electrochemical impedance spectroscopy (EIS) spectra were collected. FFA was used to estimate the production of $^1O_2$ in the systems. BA was used to estimate the production of •OH in the systems. NBT method was used to estimate the production of $^{\bullet}O_2^-$ in the systems. Estimating the production of H_2O_2 in the system using the iodometric method. The surface element compositions and valence states of the samples were obtained by X-ray photoelectron

spectroscopy (XPS, Thermo Scientific ESCALAB Xi^+). The Agilent 7700 (USA) utilized ICP-MS to evaluate the amount of Fe and Cu ions that leached from the a-FeOOH-Cu^0/Air system. UPLC-MS (Ultimate 3000, Thermo Scientific, USA) was employed to identify the degradation intermediates, X-ray absorption spectroscopy data were collected at the BL14W1 station in Shanghai Synchrotron Radiation Facility (SSRF).

Text S3 Kinetic model.

The catalytic reaction kinetics were simulated by using a pseudo-primary kinetic model (Eq. (S1)).

$$\ln(\frac{C}{C_0}) = -k_{obs} \bullet t \quad \text{(S1)}$$

where C denotes the concentration of the pollutant at time t (min), C_0 is the initial concentration (mg/L), and the k_{obs} value is the rate constant (min^{-1}) for a pseudo-primary kinetic model of the degradation process.

Text S4 The Langmuir−Hinshelwood model.

The Langmuir-Hinshelwood model (Eq. (S2)), which has been widely used to describe heterogeneous catalytic reactions, was used to obtain the adsorption coefficient of OTC on catalyst, k_L (L/mg), and the reaction rate constant of adsorbed OTC, k_r (mg/(L·min))

$$r_0 = \frac{k_r \times k_L \times C_0}{1 + k_L \times C_0} \quad \text{(S2)}$$

where r_0 (mg/(L·min)) is the reaction rate at concentration C_0 ($r_0 = k_{obs} \times C_0$).

Text S5 LCA analysis.

In this study, we built a model using Simapro 9.4.0.1 and the data Ecoinvtent3.9.1 and quantified it using ReCiPe 2016 Midpoint (H)V1.07/World (2010). We assessed the environmental impacts of treating 1 ton of wastewater through three different processes: the Fe^{2+}+H_2O_2/ Fenton system, a-FeOOH-Cu^0/PMS system, and the a-FeOOH-Cu^0/air system.

Text S6 Synchrotron Radiation analysis.

X-ray absorption spectroscopy data were collected at the BL14W1 station in Shanghai Synchrotron Radiation Facility (SSRF).

Cu elemental analysis

The obtained XAFS data was processed in Athena (version 0.9.26) (Ravel and Newville, 2005) for background, pre-edge line and post-edge line calibrations. Then Fourier transformed fitting was carried out in Artemis (version 0.9.26) (Ravel and Newville, 2005). The k^2 weighting, k-range of 3-~12 $Å^{-1}$ and R range of 1-3 Å were used for the fitting of Cu-foil; The k^2 weighting, k-range of 3-~12 $Å^{-1}$ and R range of 1-3 Å were used for the fitting of Cu-Sample.

For Wavelet Transform analysis, the χ(k) exported from Athena was imported into the Hama Fortran code. The parameters were listed as follow: R range, 0-4 Å; k range, 0-16 $Å^{-1}$; k weight, 2; and Morlet function with κ=10, σ=1 was used as the mother wavelet to provide the overall distribution.

Fe elemental analysis

The obtained XAFS data was processed in Athena (version 0.9.26) (Ravel and Newville, 2005) for background, pre-edge line and post-edge line calibrations. Then Fourier transformed fitting was carried out in Artemis (version 0.9.26) (Ravel and Newville, 2005). The k^2 weighting, k-range of 3-~12.5 $Å^{-1}$ and R range of 1-3 Å were used for the fitting of Fe-foil; The k^2 weighting, k-range of 3-~12.5 $Å^{-1}$ and R range of 1-3 Å were used for the fitting of Fe-Sample.

For Wavelet Transform analysis, the χ(k) exported from Athena was imported into the Hama Fortran code. The parameters were listed as follow: R range, 0-4 Å; k

range, 0-16 $Å^{-1}$; k weight, 2; and Morlet function with $\kappa=10$, $\sigma=1$ was used as the mother wavelet to provide the overall distribution.

Text S7 DFT calculation.

Geometry optimizations were performed using DFT (Kresse and Furthmüller, 1996b,a) as implemented in the Vienna Ab initio Simulation Package. The exchange-correlation interactions were described by the Perdew-Burke-Ernzerhof generalized gradient approximation (Perdew et al., 1996). Electron-ion interactions were treated using the projector augmented-wave method (Blöchl, 1994; Kresse and Joubert, 1999), with a plane-wave kinetic energy cutoff of 450 eV. Convergence thresholds were set to 10^{-5} eV for electronic self-consistency and 0.04 eV/Å for ionic relaxation. A vacuum spacing of 20 Å was applied normal to the surface plane, and van der Waals interactions were corrected using Grimme's DFT-D3 method(Grimme et al., 2010). A 2×2×1 Monkhorst-Pack k-point mesh was used for Brillouin-zone integration during structural relaxation.

Text S8 Quantifying the steady-state concentration and contribution of ROSs.

BA functions as a chemical probe for •OH, as it can be oxidized by •OH to yield HBA (Lu et al., 2019). NBT can be used to detect superoxide anions ($^{\bullet}O_2^-$) and exhibits a maximum absorption peak at a wavelength of 259 nm (Guo et al., 2020). Meanwhile, FFA functions as a chemical probe for $^1O_2$, as it can be degraded by $^1O_2$, $^{\bullet}O_2^-$ and •OH (Ren et al., 2025).

The probe compounds BA (10mg/L), FFA (100 μmol/L), and NBT (100 μmol/L) are at concentration levels that would not affect degradation of OTC. The steady-state concentrations of •OH, $^1O_2$ (over-rated), and $^{\bullet}O_2^-$ can be obtained by the following equations:

$$-\frac{\mathrm{d[BA]}}{\mathrm{d}t} = k_{\mathrm{BA,\bullet OH}}\,[\bullet\mathrm{OH}]\,[\mathrm{BA}] \quad \text{(S3)}$$

(BA can quench •OH)

$$-\frac{\mathrm{d[NBT]}}{\mathrm{d}t} = k_{\mathrm{NBT},\,^{\bullet}O_2^-}\,[^{\bullet}O_2^-]\,[\mathrm{NBT}] \quad \text{(S4)}$$

(NBT can quench $^{\bullet}O_2^-$)

$$-\frac{\mathrm{d[FFA]}}{\mathrm{d}t} = k_{\mathrm{FFA},\,^{\bullet}O_2^-}\,[^{\bullet}O_2^-]\,[\mathrm{FFA}] + k_{\mathrm{FFA,\bullet OH}}\,[\bullet\mathrm{OH}]\,[\mathrm{FFA}] + k_{\mathrm{FFA},\,^1O_2}\,[^1O_2]\,[\mathrm{FFA}] \quad \text{(S5)}$$

(FFA can quench $^1O_2$, •OH and $^{\bullet}O_2^-$)

Integrating Equations (S3-5) gives

$$-\ln\frac{[\mathrm{BA}]}{[\mathrm{BA}]_0} = k_{\mathrm{BA,\bullet OH}}\,[\bullet\mathrm{OH}]_{\mathrm{ss}}\,t = k_{\mathrm{obs,\,BA}}\,t \quad \text{(S6)}$$

$$-\ln\frac{[\mathrm{NBT}]}{[\mathrm{NBT}]_0} = k_{\mathrm{NBT},\,^{\bullet}O_2^-}\,[^{\bullet}O_2^-]_{\mathrm{ss}}\,t = k_{\mathrm{obs,\,NBT}}\,t \quad \text{(S7)}$$

$$-\ln\frac{[\mathrm{FFA}]}{[\mathrm{FFA}]_0} = (k_{\mathrm{FFA},\,^{\bullet}O_2^-}\,[^{\bullet}O_2^-]_{\mathrm{ss}} + k_{\mathrm{FFA,\bullet OH}}\,[\bullet\mathrm{OH}]_{\mathrm{ss}} + k_{\mathrm{FFA},\,^1O_2}\,[^1O_2]_{\mathrm{ss}})\,t = k_{\mathrm{obs,\,FFA}}\,t \quad \text{(S8)}$$

[BA], [NBT], and [FFA] are the concentrations of BA, NB, and FFA at time t, respectively. $[BA]_0$, $[NBT]_0$, and $[FFA]_0$ are the initial concentrations of BA, NB, and FFA, respectively. $k_{\mathrm{BA,\bullet OH}}$ (5.9×10^9 $M^{-1}s^{-1}$) is the second-order rate constants of •OH

with BA, respectively. $k_{NBT,\ ^{\bullet}O_2^-}$ is the second-order rate constant of NBT with $^{\bullet}O_2^-$ ($5.88 \times 10^4\ M^{-1}s^{-1}$). $k_{FFA,\ \bullet OH}$ ($3.6 \times 10^9\ M^{-1}s^{-1}$), $k_{FFA,\ ^{\bullet}O_2^-}$ ($3.5\times10^3\ M^{-1}s^{-1}$) and $k_{FFA,\ ^1O_2}$ ($1.2 \times 10^8\ M^{-1}s^{-1}$) are the second-order rate constants of •OH $^{\bullet}O_2^-$ and $^1O_2$ with FFA, respectively. $[\bullet OH]_{ss}$ is the steady-state concentrations of •OH. notably, $[^1O_2]_{ss}$, over is the overrated steady-state concentration of $^1O_2$. $[species]_{ss}$ is the steady-state concentrations of •OH, $^{\bullet}O_2^-$, and overrated $^1O_2$. The pseudo-first-order rate constants of BA ($k_{obs,BA}$), NBT ($k_{obs,NBT}$), FFA ($k_{obs,FFA}$) can be obtained from linear fitting of $ln\frac{[BA]}{[BA]_0}$, $ln\frac{[NBT]}{[NBT]_0}$,and $ln\frac{[FFA]}{[FFA]_0}$ versus time, respectively.

Text S9 Calculations of relative contribution of the reactive species.

The comparison of k_{obs} values obtained with and without quenchers, combined with quantitative evaluation of individual ROS contributions derived from these values (Li et al., 2021), allows for clear elucidation of the respective roles played by different active species in the reaction.

The relative contributions of different reactive species can be calculated as:

$$\alpha(^1O_2) = \frac{k_{CK} - k_{TEMP}}{k_{CK}} \quad \text{(S9)}$$

$$\alpha(\bullet OH) = \frac{k_{CK} - k_{TBA}}{k_{CK}} \quad \text{(S10)}$$

$$\alpha(^{\bullet}O_2^-) = \frac{k_{CK} - k_{p-BQ}}{k_{CK}} \quad \text{(S11)}$$

$$\beta(^1O_2) = \frac{\alpha(^1O_2)}{\alpha(^1O_2)+\alpha(\bullet OH)+\alpha(^{\bullet}O_2^-)} \quad \text{(S12)}$$

$$\beta(\bullet OH) = \frac{\alpha(\bullet OH)}{\alpha(^1O_2)+\alpha(\bullet OH)+\alpha(^{\bullet}O_2^-)} \quad \text{(S13)}$$

$$\beta(^{\bullet}O_2^-) = \frac{\alpha(^{\bullet}O_2^-)}{\alpha(^1O_2)+\alpha(\bullet OH)+\alpha(^{\bullet}O_2^-)} \quad \text{(S14)}$$

Where α and β are the decreased reaction kinetic constant efficiencies and the relative contributions of the reactive species to OTC degradation, respectively. k_{CK} is the reaction kinetic constant without the scavengers. k_{TEMP}, k_{TBA}, $k_{p\text{-}BQ}$ are the reaction kinetic constants in the presence of TEMP, TBA, p-BQ, respectively.

Text S10 The adsorption energy (E) of O_2 on Fe and Cu.

$$E_{ads}=E_{m/slab}-E_m-E_{slab} \quad (S15)$$

where E_{ads} is the energy of adsorption, $E_{m/slab}$ is the energy of the whole system after adsorption, E_m is the energy of the adsorbed molecule, and E_{slab} is the energy of the surface model before adsorption.

Text S11 Cost calculation

We calculated the prices of the reagents used in the experiment by consulting reagent websites such as Macklin and Aladdin. The results indicate that the price of iron(III) nitrate nonahydrate is approximately \$0.0101 per gram, ammonium bicarbonate about \$0.0062 per gram, anhydrous copper sulfate about \$0.0109 per gram, sodium borohydride about \$0.5726 per gram, and anhydrous ethanol about \$0.0025 per gram. In this study, 0.404 grams of iron(III) nitrate nonahydrate, 0.2372 grams of ammonium bicarbonate, 78.93 grams of anhydrous ethanol, 0.1596 grams of anhydrous copper sulfate, and 0.1892 grams of sodium borohydride were used to synthesize approximately 0.1524 grams of a-FeOOH-Cu^0 material. The calculated reagent cost is about \$2.05 per gram. The magnetic stirrer has a power of 0.04 kW and operated for 9 hours, consuming 0.36 kWh of electricity, resulting in an electricity cost of \$0.029. Overall, the comprehensive cost of the a-FeOOH-Cu^0 material is approximately \$2.079 per gram. This cost analysis demonstrates that our synthesis method is economically feasible, providing valuable cost data for subsequent experimental research and applications. The analysis confirms the cost-effectiveness

of the synthesis approach we employed. Improvements in factors such as reaction conditions, material availability, and yield could further enhance the industrial viability of this process. The initial cost is not prohibitively high, and over time, economies of scale and technological advancements may lead to cost reductions, indicating potential for future industrial production.

Table S1 BET surface area for various catalysts.

Catalyst	BET surface area (m^2/g)
a-FeOOH	268.7502
a-FeOOH-Cu^0	49.4509

Table S2 EXAFS fitting parameters at the Cu K-edge for various samples.

	shell	CN[a]	R[b](Å)	σ^{2c}(Å^2)	ΔE_0[d](eV)	R factor
Cu-foil	Cu-Cu	12	2.54±0.01	0.0086	4.2±0.6	0.0037
a-FeOOH-Cu^0	Cu-O	2.1±0.4	2.11±0.03	0.0094	3.5±1.8	0.0099
	Cu-Cu	6.4±0.3	2.54±0.01	0.0081		

[a]CN: coordination numbers; [b]R: bond distance; [c]σ^2: Debye-Waller factors; [d]ΔE_0: the inner potential correction. R factor: goodness of fit.

Table S3 EXAFS fitting parameters at the Fe K-edge for various samples.

	shell	CN[a]	R[b](Å)	σ²[c](Å²)	ΔE₀[d](eV)	R factor
Fe-foil	Fe-Fe1	8	2.47±0.01	0.0060	5.0±2.1	0.0067
	Fe- Fe2	6	2.84±0.01	0.0058		
a-FeOOH-Cu⁰	Fe-O	5.80±0.3	1.94±0.01	0.0079	-6.8±1.9	0.0113
	Fe-O-Fe1	4.28±1.2	3.02±0.02	0.0069		
	Fe-O-Fe2	3.75±0.8	3.41±0.02	0.0073		

[a]CN: coordination numbers; [b]R: bond distance; [c]σ^2: Debye-Waller factors; [d]ΔE_0: the inner potential correction. R factor: goodness of fit. Error bounds that characterize the structural parameters obtained by EXAFS spectroscopy were estimated as CN±20%; R±1%; σ^2±20%.

Table S4 The pseudo-first-order kinetic constants and initial reaction rates of OTC at different initial concentrations.

catalyst	C_0 (mg/L)	k_{obs} (min^{-1})	r_0 (mg/(L·min))
Cu⁰	5	0.1295	0.6475
	10	0.1137	1.1370
	20	0.0429	0.8580
a-FeOOH	5	0.0675	0.3375
	10	0.0750	0.7500
	20	0.0399	0.7980
a-FeOOH-Cu⁰	5	0.4499	2.2495
	10	0.3231	3.2310
	20	0.1991	3.9820

Table S5 The leaching Cu and Fe concentrations in a-FeOOH-Cu⁰/air system.

Element	Single cycle (mg/L)	Five cycles (mg/L)
Fe	0.00656	0.00273
Cu	0.16295	0.12375

Table S6 Comparison of different materials for O_2 activation to degrade pollutants.

Catalyst	Pollutant	Reaction Conditions	Removal efficiency (%)	Reference
$BiOBr/FeMoO_4$	OTC	[pollutant] = 20 mg/L, [catalyst] = 200 mg/L, [PDS] = 2 mM, pH = 6	96.8	(Xi et al., 2025)
Bi_2WO_6/C-TiO_2	OTC	[pollutant] = 15 mg/L, [catalyst] = 0.30 g/L, pH = 7	93.6	(Shi et al., 2024)
Z-scheme γ-Fe_2O_3/g-C_3N_4	OTC	[pollutant] = 20 mg/L, [catalyst] = 1.00 g/L, [Temperature] = 25 ℃, pH = 5	85.7	(Yang et al., 2025)
MAC	OTC	[pollutant] = 20 mg/L, [catalyst] = 100 mg/L, [PMS] = 0.5mM, pH = 6.8 ± 0.15	100	(Di et al., 2024)
KB/BMO-GO	OTC	[pollutant] = 50 mg/L, [catalyst] = 0.4 g/L, pH = 7	81.6	(Zhang et al., 2024b)
BCBF-OV2	OTC	[pollutant] = 10 mg/L, [catalyst] = 2.00 g/L, pH = 5.8	91.9	(Xie et al., 2025)
C1M5	OTC	[pollutant] = 5 mg/L, [catalyst] = 100 mg/L, [PS] = 2.0 mM, pH = 4.55	89.3	(Zhang et al., 2025)
Cu^0-F-MoS_2	OTC	[pollutant] = 10 mg/L, [catalyst] = 100 mg/L, [bubbling air] = 2 L/min, pH = 6.0 ± 0.1, T = 298 K	90.0	(Zheng et al., 2025)
ACS-3	OTC	[pollutant] = 50 mg/L, [Catalyst] = 50 mg/L, [PDS] = 1 mM, T = 25 ◦C	96.2	(Guo et al., 2025)
LBC-40	OTC	[pollutant] = 20 mg/L, [Catalyst] = 1.00 g/L, pH = 6	85.28	(Zhang et al., 2024a)
Co/C-3	OTC	[pollutant] = 10 mg/L, [Catalyst] = 200 mg/L, [H_2O_2] = 1	100	(Hong et al., 2021)

		mM, pH = 7		

Table S7 Functional groups content of a-FeOOH-Cu^0 before and after reaction.

Catalyst		Before (%)	After (%)
Cu^0	Cu^0/Cu^+	82.8	
	Cu^{2+}	17.2	
a-FeOOH	Fe^{2+}	65.3	
	Fe^{3+}	34.7	
	Ovs	69.3	
	Fe-O	30.7	
a-FeOOH-Cu^0	Cu^0/Cu^+	67.1	
2:1	Cu^{2+}	32.9	
	Fe^{2+}	61.3	
	Fe^{3+}	38.7	
	Ovs	71.1	
	Fe-O	28.9	
a-FeOOH-Cu^0	Cu^0/Cu^+	65.5	
2:1.5	Cu^{2+}	34.5	
	Fe^{2+}	69.9	
	Fe^{3+}	30.1	
	Ovs	85.7	
	Fe-O	14.3	
a-FeOOH-Cu^0	Cu^0/Cu^+	80.3	57.5
2:2	Cu^{2+}	19.7	42.5
	Fe^{2+}	69.1	62.9
	Fe^{3+}	30.9	37.1
	Ovs	65.6	74.9
	Fe-O	34.4	25.1
a-FeOOH-Cu^0	Cu^0/Cu^+	43.3	
2:3	Cu^{2+}	56.7	
	Fe^{2+}	68.5	
	Fe^{3+}	31.5	
	Ovs	86.2	
	Fe-O	13.8	
a-FeOOH-Cu^0	Cu^0/Cu^+	71.4	
2:4	Cu^{2+}	28.6	
	Fe^{2+}	73.5	
	Fe^{3+}	26.5	
	Ovs	67.6	
	Fe-O	32.4	

Table S8 Impact assessment for the treatment of 1 ton OTC wastewater (Fe^{2+}+H_2O_2 system).

			$FeSO_4 \cdot 7H_2O$	H_2O_2	Generated sludge, dry base	Power supply	Stirrer
Impact category	Unit	Total	Iron sulfate {RoW| market for iron sulfate | Cut-off, S	Hydrogen peroxide, without water, in 50% solution state{RoW | market for hydrogen peroxide, without water, in 50% solution state | Cut-off, S	Sewage sludge, dried {RoW | market for sewage sludge, dried | Cut-off, U	Electricity, high voltage {CN | market group for | Cut-off, S	Electricity, high voltage {CN | market group for | Cut-off, S
Global warming	kg CO_2 eq	19.47646	4.206564	0.768247	0.014072363	9.380444	5.107131
Stratospheric ozone depletion	kg CFC11 eq	4.93E-06	1.67E-06	2.19E-07	5.03E-09	1.96E-06	1.07E-06
Ionizing radiation	kBq Co-60 eq	0.560193	0.310826	0.027722	0.000683232	0.143069	0.077893
Ozone formation, Human health	kg NO_x eq	0.056639	0.014813	0.001545	1.74E-05	0.02607	0.014194
Fine particulate matter formation	kg PM2.5 eq	0.033849	0.010538	0.00117	1.41E-05	0.014326	0.0078
Ozone formation, Terrestrial ecosystems	kg NO_x eq	0.056987	0.015009	0.001612	1.77E-05	0.026125	0.014224

Terrestrial acidification	kg SO_2 eq	0.071972	0.020319	0.002296	2.48E-05	0.031941	0.01739
Freshwater eutrophication	kg P eq	0.005616	0.002424	0.000517	2.96E-06	0.00173	0.000942
Marine eutrophication	kg N eq	0.000346	0.000126	4.90E-05	2.03E-07	0.00011	6.01E-05
Terrestrial ecotoxicity	kg 1,4-DCB	63.52907	52.16601	3.392086	0.013686212	5.1522	2.805087
Freshwater ecotoxicity	kg 1,4-DCB	0.740949	0.553724	0.045459	0.000355917	0.091561	0.04985
Marine ecotoxicity	kg 1,4-DCB	0.980411	0.723661	0.06051	0.000456416	0.126767	0.069018
Human carcinogenic toxicity	kg 1,4-DCB	1.064662	0.527612	0.096668	0.000375988	0.284896	0.15511
Human non-carcinogenic toxicity	kg 1,4-DCB	17.14432	9.735482	0.983401	0.005604436	4.156728	2.263107
Land use	m^2a crop eq	0.367789	0.18174	0.012973	0.000204897	0.111931	0.06094
Mineral resource scarcity	kg Cu eq	0.049441	0.042823	0.002137	2.20E-05	0.002887	0.001572
Fossil resource scarcity	kg oil eq	4.143762	1.084234	0.232505	0.003384458	1.828255	0.995383
Water consumption	m^3	0.099823	0.026397	0.037519	5.43E-05	0.023214	0.012639

Calculation:	Analyze
Results:	Impact assessment
Product:	Treatment of 1 ton OTC wastewater (Fe^{2+}+H_2O_2 system).
Method:	ReCiPe 2016 Midpoint (H) V1.07 / World (2010) H
Indicator:	Characterization
Skip categories:	Never
Exclude infrastructure processes:	No
Exclude long-term emissions:	No
Sorted on item:	Impact category
Sort order:	Ascending

Table S9 Impact assessment for the treatment of 1 ton OTC wastewater (a-FeOOH-Cu^0/PMS system).

			$CuSO_4$	$Fe(NO_3)_3·9H_2O$	$NaBH_4$	PMS	N_2	Power supply	Stirrer	Centrifuge	Percentage difference
Impact category	Unit	Total	Copper sulfate {GLO | market for | Cut-off, S	Iron(III) nitrate, without water, in 14% iron solution state {GLO | market for | Cut-off, S	Sodium borohydride, powder {GLO | market for | Cut-off, S	Sodium persulfate {GLO | market for | Cut-off, S	Nitrogen, liquid {RoW | market for | Cut-off, S	Electricity, high voltage {CN | market group for | Cut-off, S	Electricity, high voltage {CN | market group for | Cut-off, S	Electricity, high voltage {CN | market group for | Cut-off, S	Compare with Fe^{2+}+H_2O_2 system
Global warming	kg CO_2 eq	3.288761	0.152328	0.019628	0.290438	0.009616	0.002619	0.521136	2.18877	0.104227	17%
Stratospheric ozone depletion	kg CFC11 eq	8.88E-07	1.60E-07	1.62E-08	1.17E-07	5.64E-09	9.15E-10	1.09E-07	4.58E-07	2.18E-08	18%
Ionizing radiation	kBq Co-60 eq	0.072925	0.011968	0.004026	0.013017	0.000787	0.000206	0.007948	0.033383	0.00159	13%
Ozone formation, Human health	kg NO_x eq	0.010046	0.00119	6.30E-05	0.000939	2.61E-05	5.96E-06	0.001448	0.006083	0.00029	18%
Fine particulate matter formation	kg PM2.5 eq	0.007317	0.002384	4.67E-05	0.000554	2.89E-05	5.78E-06	0.000796	0.003343	0.000159	22%

Ozone formation, Terrestrial ecosystems	kg NO_x eq	0.010099	0.001211	6.39E-05	0.000954	2.67E-05	6.00E-06	0.001451	0.006096	0.00029	18%
Terrestrial acidification	kg SO_2 eq	0.018085	0.007337	0.000102	0.000984	7.05E-05	8.63E-06	0.001775	0.007453	0.000355	25%
Freshwater eutrophication	kg P eq	0.001415	0.000795	1.54E-05	7.77E-05	6.27E-06	1.14E-06	9.61E-05	0.000404	1.92E-05	25%
Marine eutrophication	kg N eq	5.25E-05	1.30E-05	1.03E-06	4.84E-06	4.39E-07	7.39E-08	6.13E-06	2.58E-05	1.23E-06	15%
Terrestrial ecotoxicity	kg 1,4-DCB	60.23809	57.75302	0.275291	0.49114	0.170429	0.002555	0.286233	1.20218	0.057247	95%
Freshwater ecotoxicity	kg 1,4-DCB	0.681378	0.643371	0.003168	0.005661	0.001655	5.57E-05	0.005087	0.021364	0.001017	92%
Marine ecotoxicity	kg 1,4-DCB	0.874169	0.822167	0.004129	0.0076	0.002168	7.47E-05	0.007043	0.029579	0.001409	89%
Human carcinogenic toxicity	kg 1,4-DCB	0.170374	0.070724	0.002919	0.01014	0.00102	0.000101	0.015828	0.066476	0.003166	16%
Human non-carcinogenic toxicity	kg 1,4-DCB	10.86649	9.38328	0.055923	0.145969	0.032495	0.001805	0.230929	0.969903	0.046186	63%
Land use	m^2a crop eq	0.063134	0.020509	0.000934	0.007778	0.00029	4.30E-05	0.006218	0.026117	0.001244	17%
Mineral resource scarcity	kg Cu eq	0.030232	0.028651	0.00024	0.000367	0.000107	1.44E-06	0.00016	0.000674	3.21E-05	61%

Fossil resource scarcity	kg oil eq	0.683924	0.039565	0.005084	0.087343	0.002806	0.000649	0.10157	0.426593	0.020314	17%
Water consumption	m^3	0.013335	0.004519	0.000411	0.001056	0.00032	6.43E-05	0.00129	0.005417	0.000258	13%

Calculation:	Analyze
Results:	Impact assessment
Product:	Treatment of 1 ton OTC wastewater (a-FeOOH-Cu^0/air system).
Method:	ReCiPe 2016 Midpoint (H) V1.07 / World (2010) H
Indicator:	Characterization
Skip categories:	Never
Exclude infrastructure processes:	No
Exclude long-term emissions:	No
Sorted on item:	Impact category
Sort order:	Ascending

Table S10 Impact assessment for the treatment of 1 ton OTC wastewater (a-FeOOH-Cu^0/air system).

			$CuSO_4$	$Fe(NO_3)_3 \cdot 9H_2O$	$NaBH_4$	N_2	Power supply	Stirrer	Centrifuge	Percentage difference
Impact category	Unit	Total	Copper sulfate {GLO | market for | Cut-off, S	Iron(III) nitrate, without water, in 14% iron solution state {GLO | market for | Cut-off, S	Sodium borohydride, powder {GLO | market for | Cut-off, S	Nitrogen, liquid {RoW | market for | Cut-off, S	Electricity, high voltage {CN | market group for | Cut-off, S	Electricity, high voltage {CN | market group for | Cut-off, S	Electricity, high voltage {CN | market group for | Cut-off, S	Compare with Fe^{2+}+H_2O_2 system
Global warming	kg CO_2 eq	1.805347	0.038082	0.004907	0.092105	0.002619	0.521136	1.042272	0.104227	9%
Stratospheric ozone depletion	kg CFC11 eq	4.31E-07	3.99E-08	4.05E-09	3.70E-08	9.15E-10	1.09E-07	2.18E-07	2.18E-08	9%
Ionizing radiation	kBq Co-60 eq	0.033766	0.002992	0.001007	0.004128	0.000206	0.007948	0.015897	0.00159	6%
Ozone formation, Human health	kg NO_x eq	0.005252	0.000298	1.58E-05	0.000298	5.96E-06	0.001448	0.002897	0.00029	9%
Fine particulate matter formation	kg PM2.5 eq	0.003336	0.000596	1.17E-05	0.000176	5.78E-06	0.000796	0.001592	0.000159	10%
Ozone formation, Terrestrial ecosystems	kg NO_x eq	0.005272	0.000303	1.60E-05	0.000302	6.00E-06	0.001451	0.002903	0.00029	9%
Terrestrial acidification	kg SO_2 eq	0.007859	0.001834	2.56E-05	0.000312	8.63E-06	0.001775	0.003549	0.000355	11%

Freshwater eutrophication	kg P eq	0.000536	0.000199	3.85E-06	2.47E-05	1.14E-06	9.61E-05	0.000192	1.92E-05	10%
Marine eutrophication	kg N eq	2.47E-05	3.24E-06	2.58E-07	1.54E-06	7.39E-08	6.13E-06	1.23E-05	1.23E-06	7%
Terrestrial ecotoxicity	kg 1,4-DCB	15.58133	14.43825	0.068823	0.155753	0.002555	0.286233	0.572467	0.057247	25%
Freshwater ecotoxicity	kg 1,4-DCB	0.179763	0.160843	0.000792	0.001795	5.57E-05	0.005087	0.010173	0.001017	24%
Marine ecotoxicity	kg 1,4-DCB	0.231595	0.205542	0.001032	0.00241	7.47E-05	0.007043	0.014085	0.001409	24%
Human carcinogenic toxicity	kg 1,4-DCB	0.072376	0.017681	0.00073	0.003216	0.000101	0.015828	0.031655	0.003166	7%
Human non-carcinogenic toxicity	kg 1,4-DCB	3.14687	2.34582	0.013981	0.04629	0.001805	0.230929	0.461859	0.046186	18%
Land use	m^2a crop eq	0.027769	0.005127	0.000234	0.002466	4.30E-05	0.006218	0.012437	0.001244	8%
Mineral resource scarcity	kg Cu eq	0.007854	0.007163	6.00E-05	0.000116	1.44E-06	0.00016	0.000321	3.21E-05	16%
Fossil resource scarcity	kg oil eq	0.364533	0.009891	0.001271	0.027699	0.000649	0.10157	0.203139	0.020314	9%
Water consumption	m^3	0.005759	0.00113	0.000103	0.000335	6.43E-05	0.00129	0.002579	0.000258	6%

Calculation: Analyze

Results: Impact assessment

Product:	Treatment of 1 ton OTC wastewater (a-FeOOH-Cu^0/PMS system).
Method:	ReCiPe 2016 Midpoint (H) V1.07 / World (2010) H
Indicator:	Characterization
Skip categories:	Never
Exclude infrastructure processes:	No
Exclude long-term emissions:	No
Sorted on item:	Impact category
Sort order:	Ascending

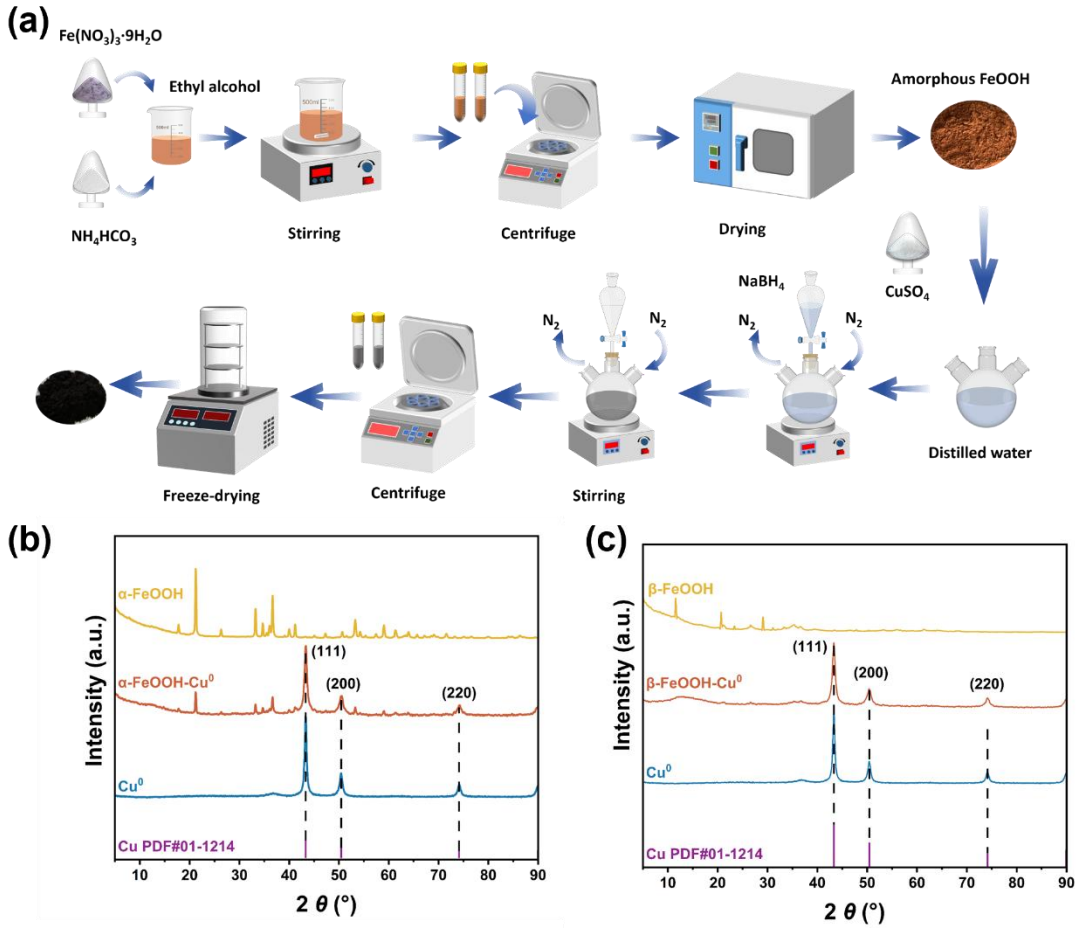

Fig. S1 (a) Preparation process of the a-FeOOH-Cu^0 catalyst, and XRD patterns of (b) Cu^0, α-FeOOH, α-FeOOH-Cu^0 and (c) Cu^0, β-FeOOH, β-FeOOH-Cu^0.

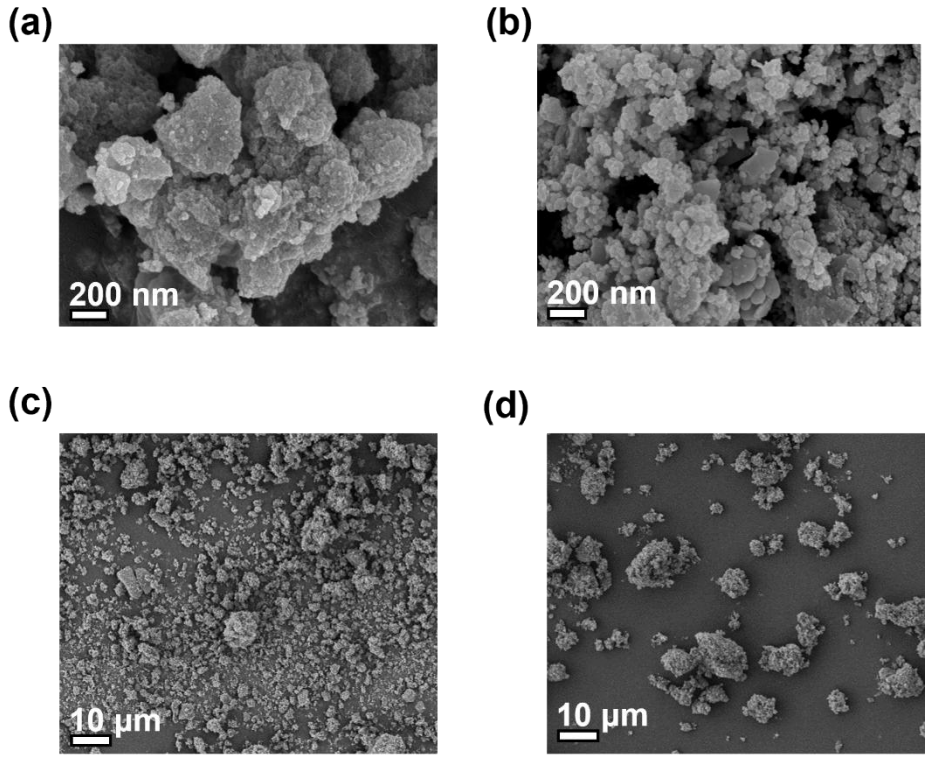

Fig. S2 SEM images of (a, c) a-FeOOH and (b, d) a-FeOOH-Cu^0.

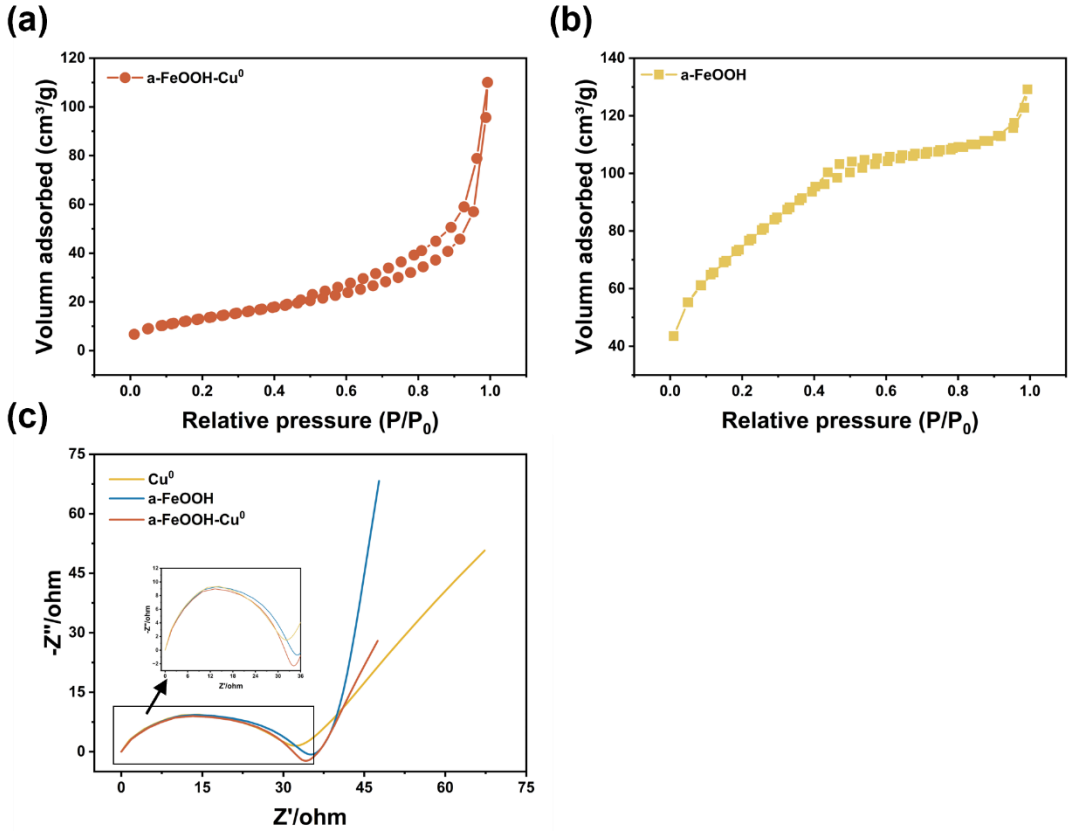

Fig. S3 N_2 adsorption-desorption isotherms of (a) a-FeOOH-Cu^0 and (b) a-FeOOH; (c) EIS of Cu^0, a-FeOOH-Cu^0 and a-FeOOH.

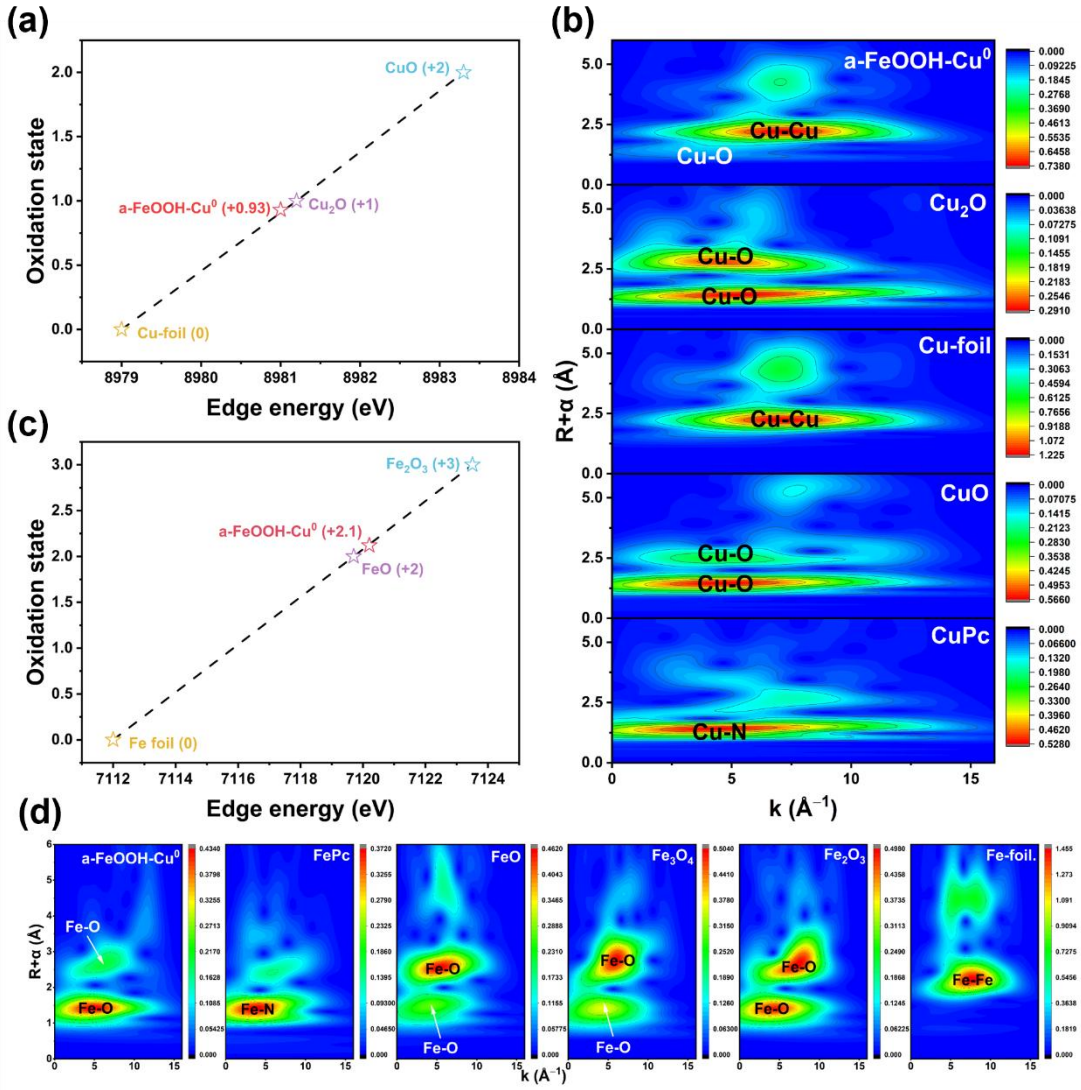

Fig. S4 Normalized Cu (a) valence state variation and (b) wavelet transform of a-FeOOH-Cu^0, Cu_2O, Cu-foil, CuO and CuPc. Normalized Fe (c) valence state variation and (d) wavelet transform of a-FeOOH-Cu^0, Fe_2O_3, Fe-foil, Fe_3O_4, FeO, and FePc.

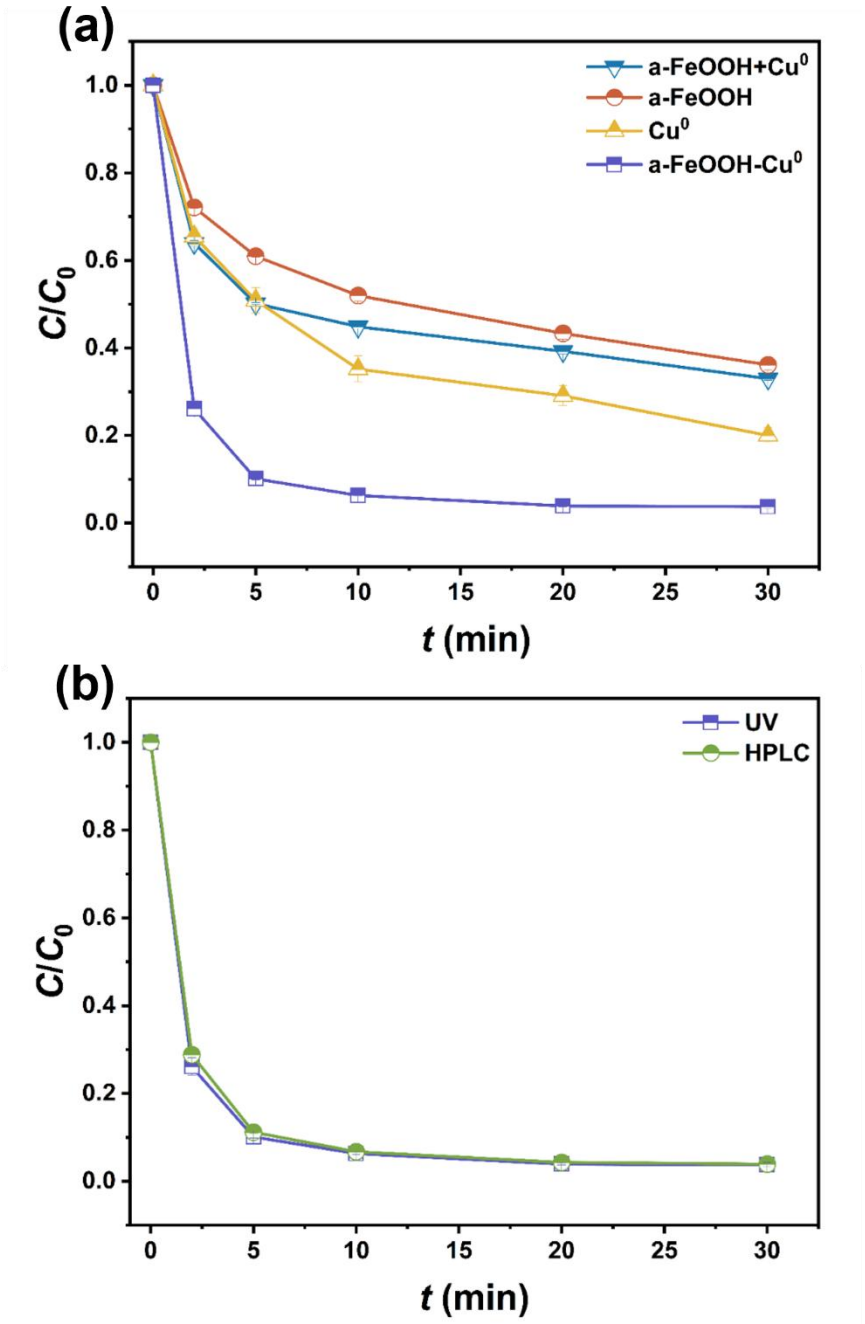

Fig. S5 (a) The effect of physically mixing a-FeOOH and Cu^0 on the degradation efficiency; (b) the degradation process of OTC by a-FeOOH-Cu^0, measured and comparatively analyzed using ultraviolet spectroscopy (UV) and high-performance liquid chromatography (HPLC).

HPLC method: 1 mL of the reaction solution filtered through a 0.45 μm membrane was transferred into a 2 mL HPLC vial for subsequent analysis. Detection

was carried out using a Shimadzu LC-20A high-performance liquid chromatography system equipped with a diode array detector. The chromatographic conditions were set as follows: mobile phase consisting of methanol and ultrapure water (volume ratio 20:80); flow rate 1.0 mL/min; column temperature 30°C; injection volume 10 μL; detection wavelength 355 nm. All samples were analyzed in triplicate, and the final results were averaged.

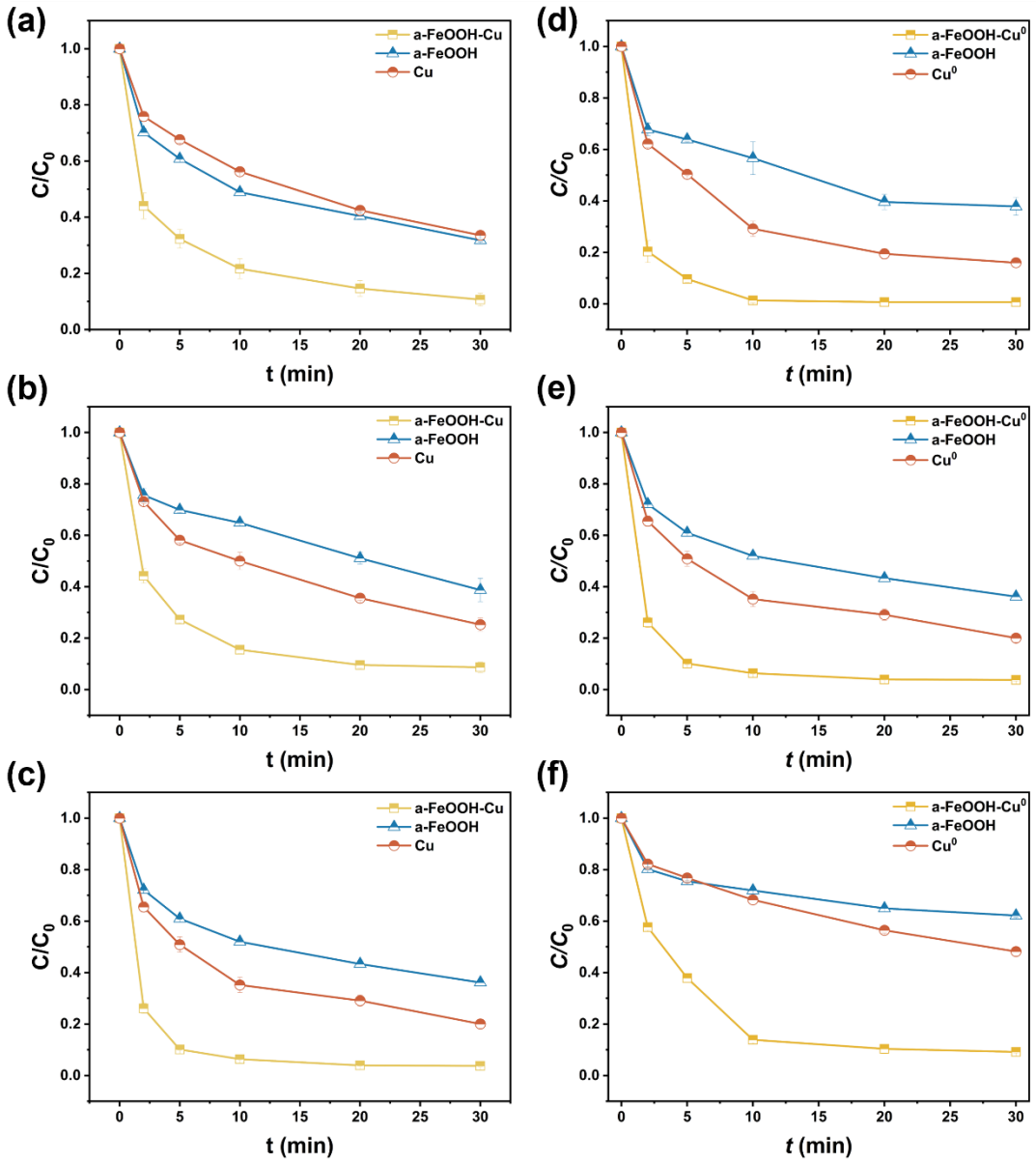

Fig. S6 The degradation effects of different catalysts at (a) pH=5, (b) pH=7, (c) pH=8, (d) OTC = 5 mg/L, (e) OTC = 10 mg/L, and (f) OTC = 20 mg/L.

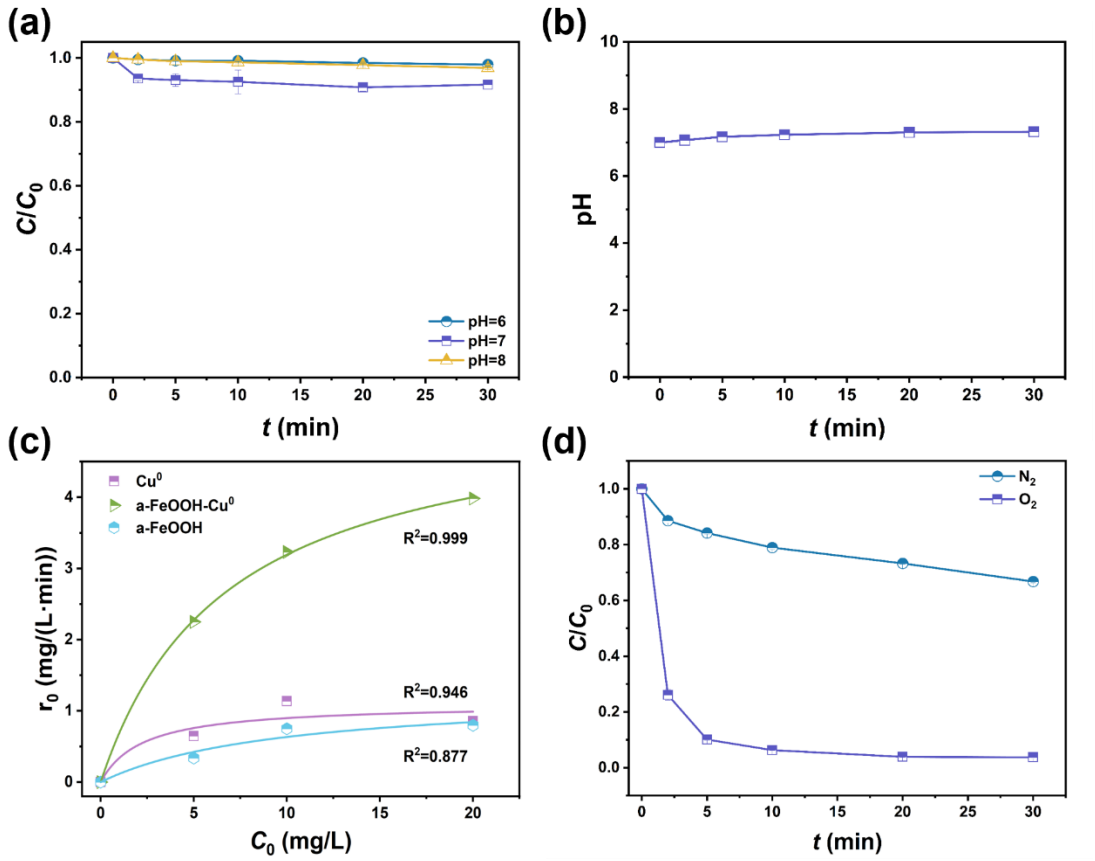

Fig. S7 (a) The degradation of OTC itself under different pH conditions; (b) the variation of pH during the reaction process; (c) fitting curves of the initial concentration (C_0) versus initial reaction rate (r_0) for OTC with different catalysts; and (d) OTC degradation efficiency by a-FeOOH-Cu^0 under N_2 and O_2 atmospheres.

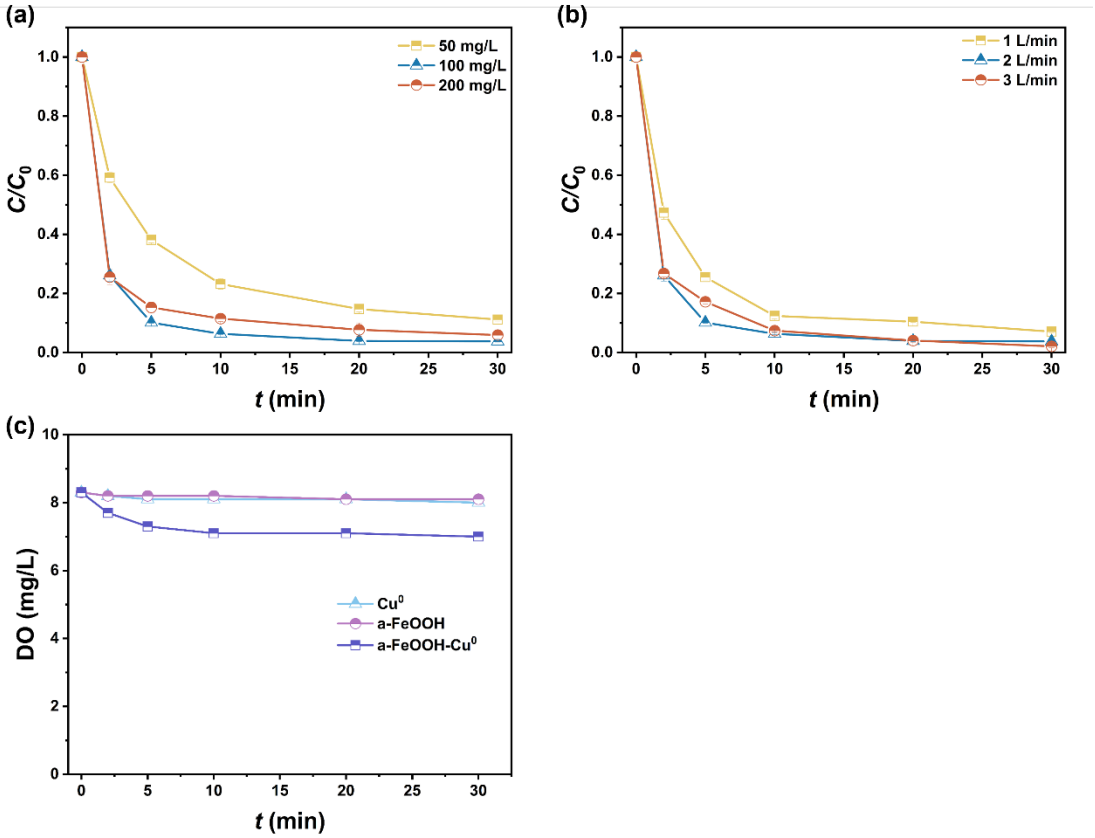

Fig. S8 OTC degradation efficiency at (a) different catalyst concentrations and (b) aeration rates; (c) variation of dissolved oxygen in different systems during the reaction.

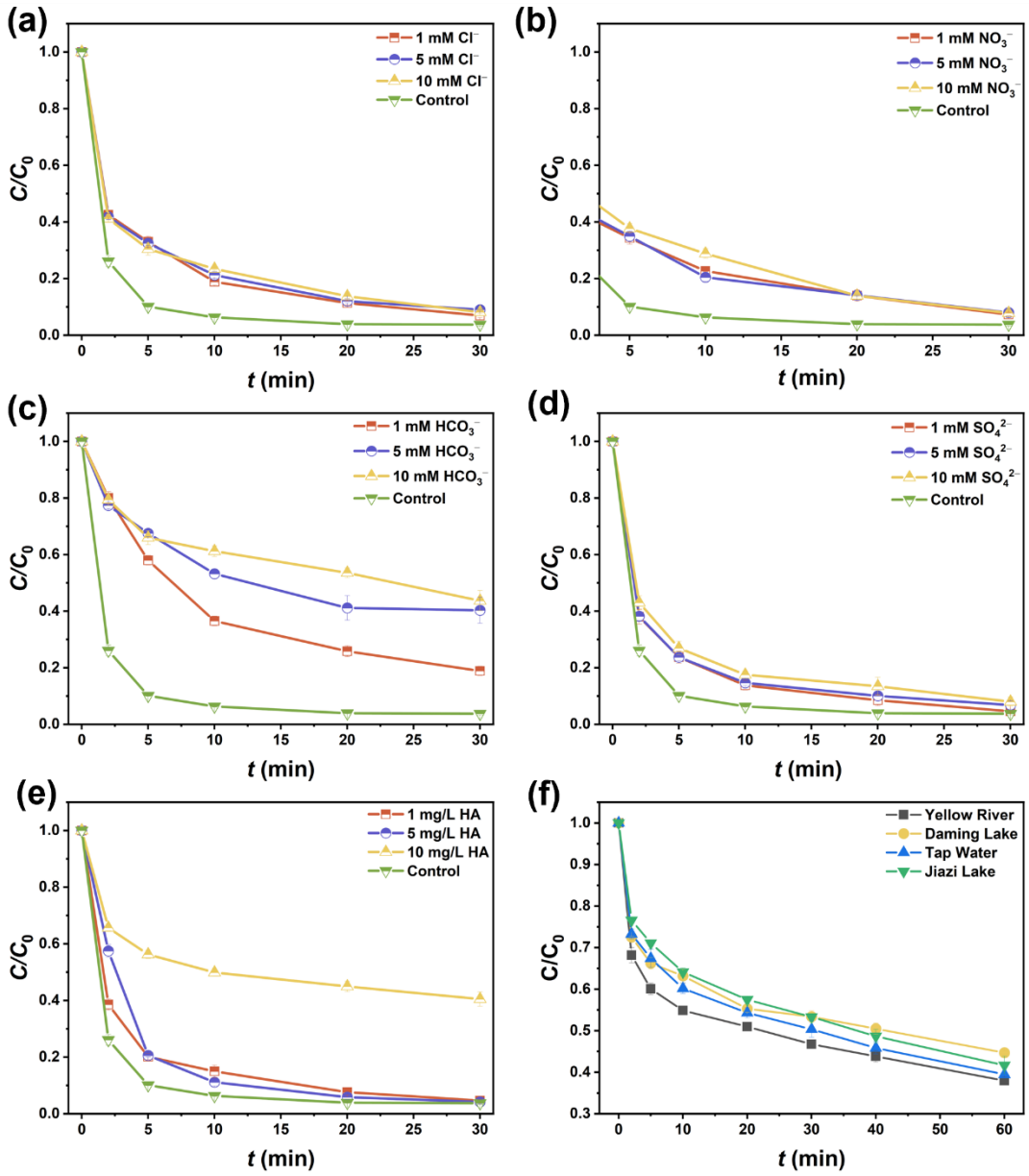

Fig. S9 The effects of different concentrations of (a) Cl^-, (b) NO_3^-, (c) HCO_3^-, (d) SO_4^{2-}, and (e) HA on the degradation of OTC; and (f) degradation effects of OTC in different actual water bodies.

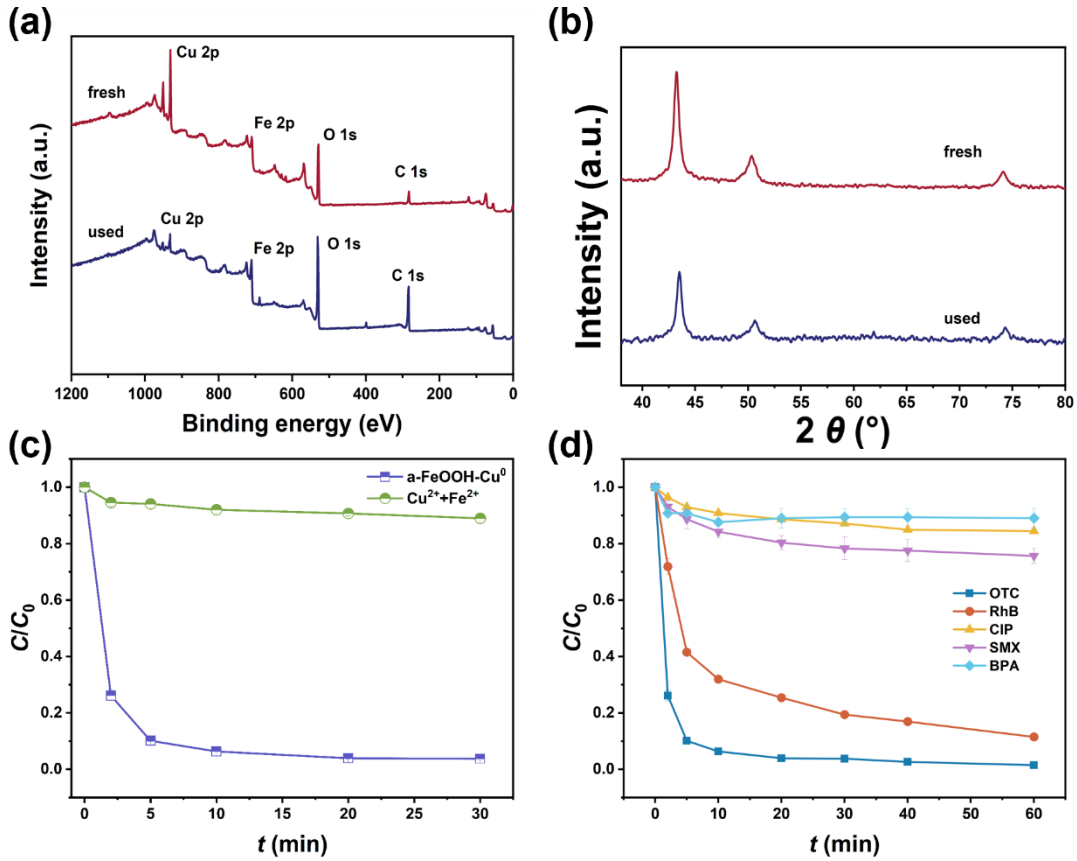

Fig. S10 (a) XPS and (b) XRD spectra of a-FeOOH-Cu^0 before and after the reaction; (c) degradation of OTC by leached ions and a-FeOOH-Cu^0; and (d) degradation of different organic compounds by a-FeOOH-Cu^0.

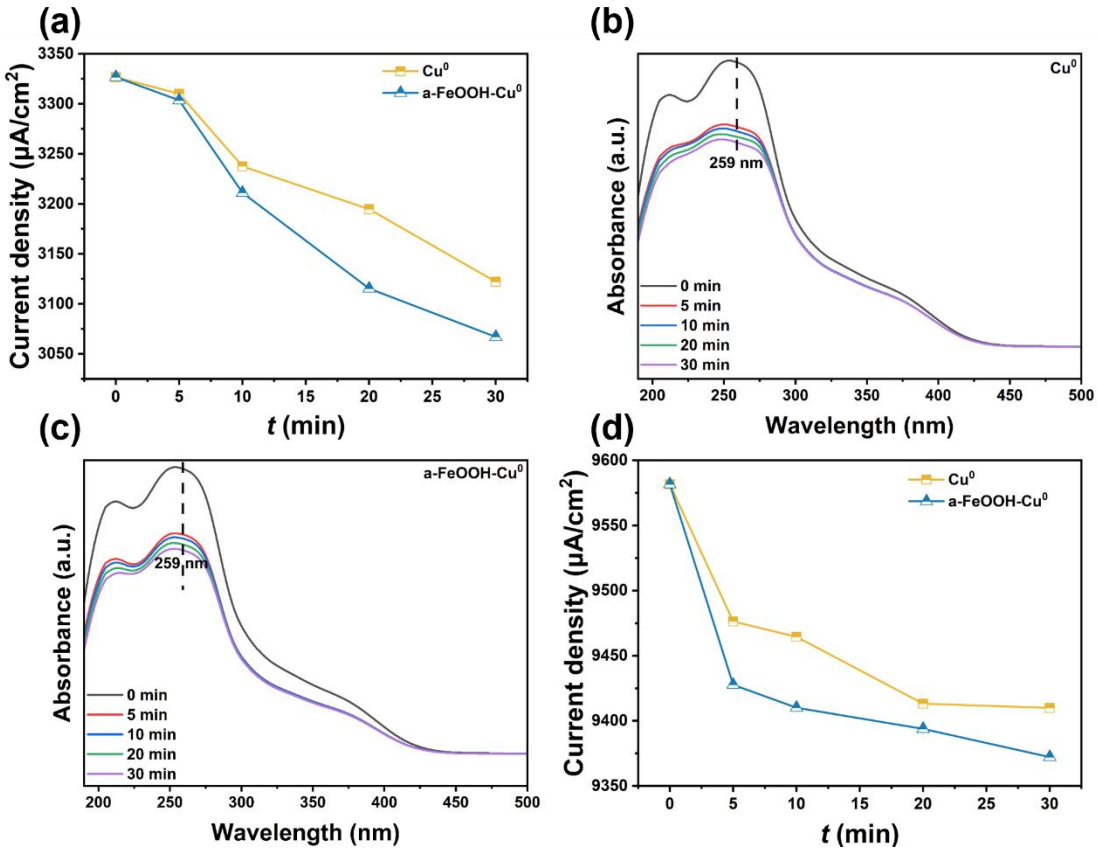

Fig. S11 (a) HPLC data showing •OH changes during the reaction processes of Cu^0 and a-FeOOH-Cu^0; spectral data showing $^{\bullet}O_2^-$ changes during the (b) Cu^0 and (c) a-FeOOH-Cu^0 reaction processes; and (d) HPLC data showing $^1O_2$ changes during the reaction processes of Cu^0 and a-FeOOH-Cu^0.

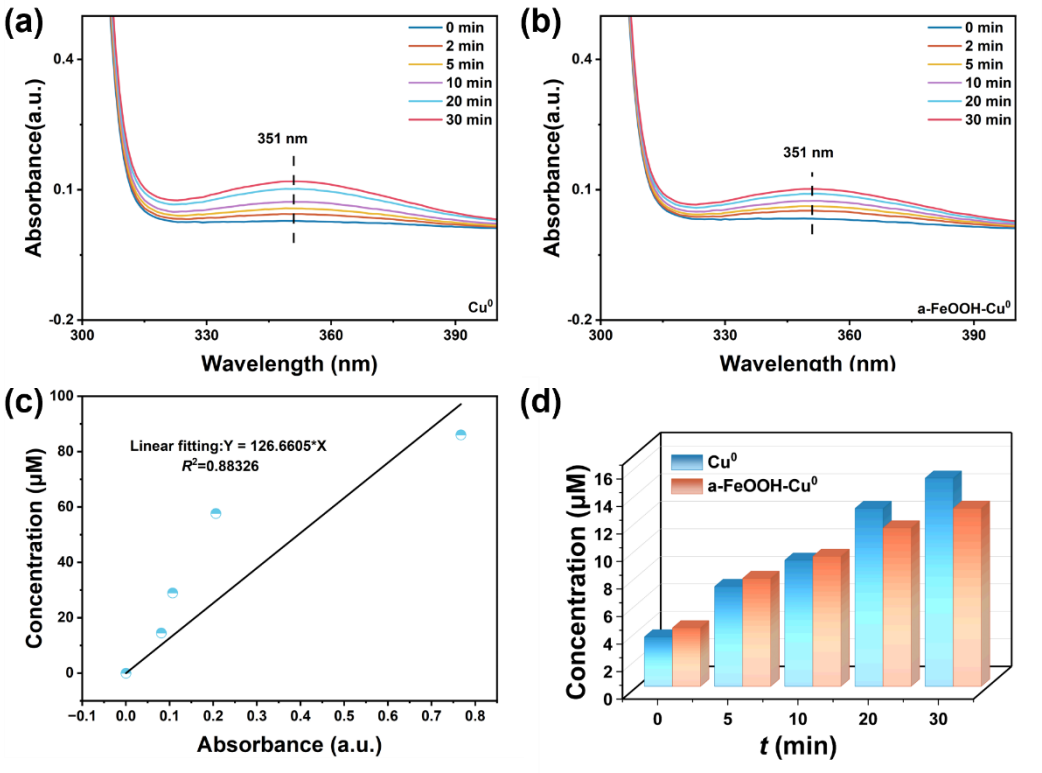

Fig. S12 (a, b) Spectral data on changes in H_2O_2 content during the reaction processes of Cu^0 and a-FeOOH-Cu^0; (c) Linear fitting spectra of H_2O_2 concentration versus absorption intensity; (d) Transient concentration of H_2O_2 in different reaction systems.

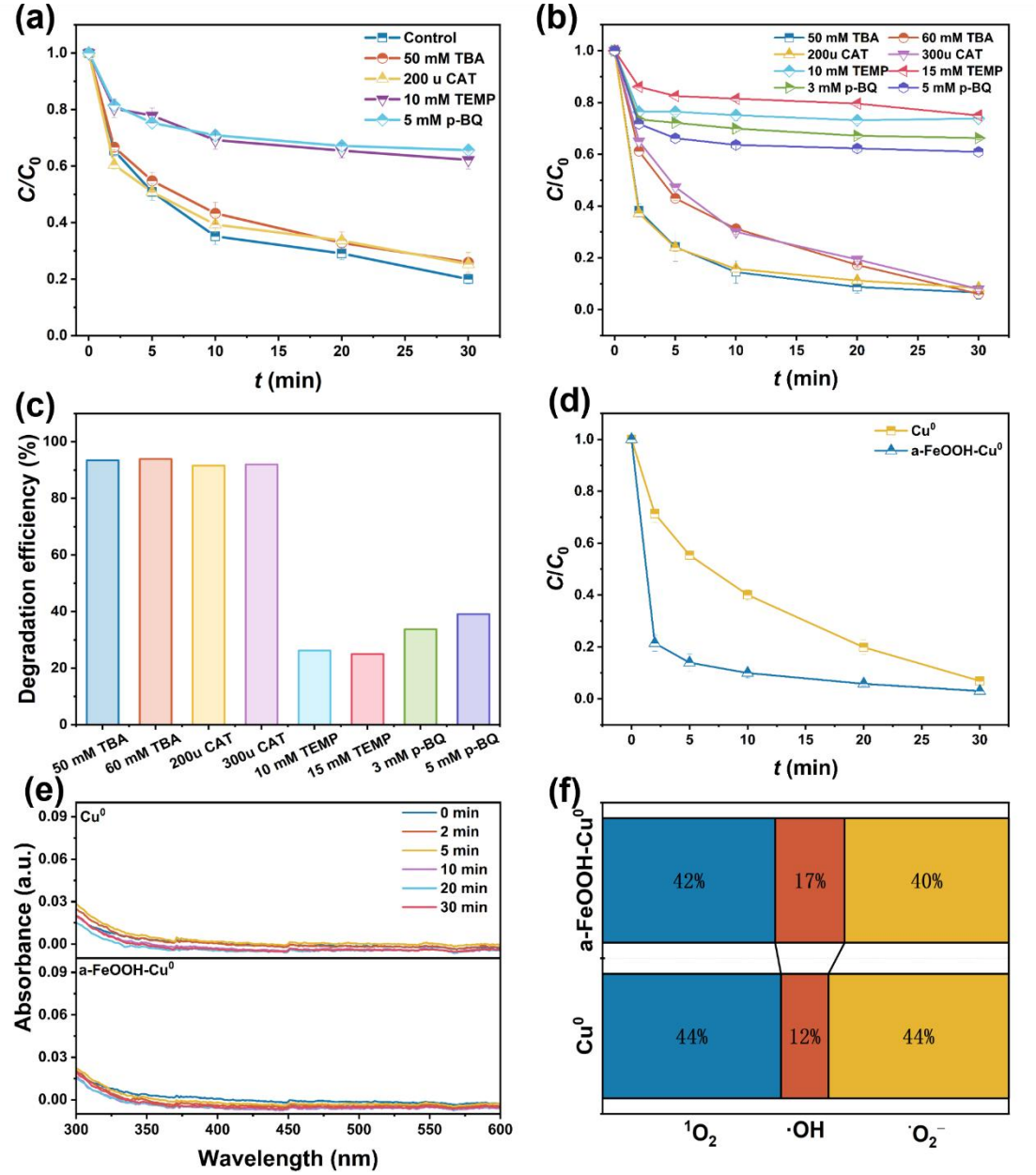

Fig. S13 Quenching experiments for the degradation of OTC by (a) Cu^0 and (b) a-FeOOH-Cu^0 with TBA, CAT, TEMP, and p-BQ, respectively; (c) the effect of different concentrations of TBA, CAT, TEMP, and p-BQ on OTC degradation efficiency; (d) the effect of high-valent metals on the catalytic degradation performance in different systems; (e) detection of high-valent copper; and (f) contribution ratios of reactive oxygen species (ROS).

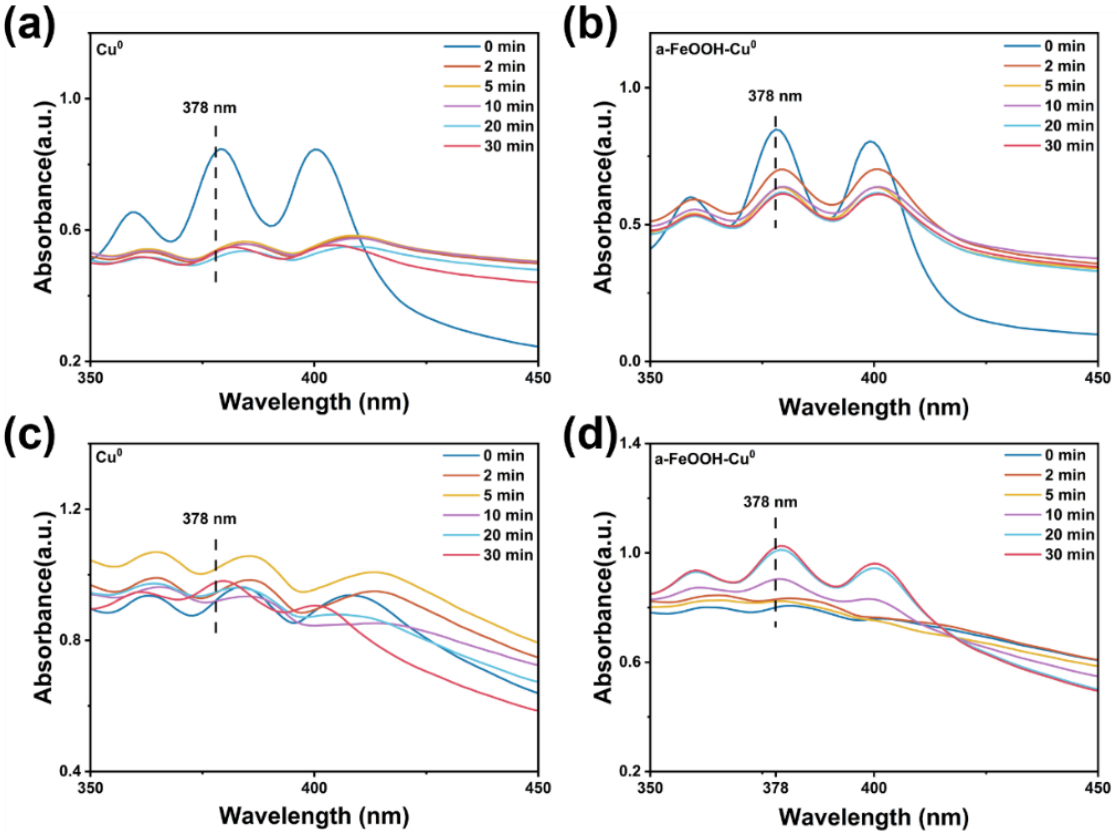

Fig. S14 Spectral data on changes in $^1O_2$ content during the Cu^0 and a-FeOOH-Cu^0 reaction processes in both the absence (a, b) and presence of p-BQ (c, d).

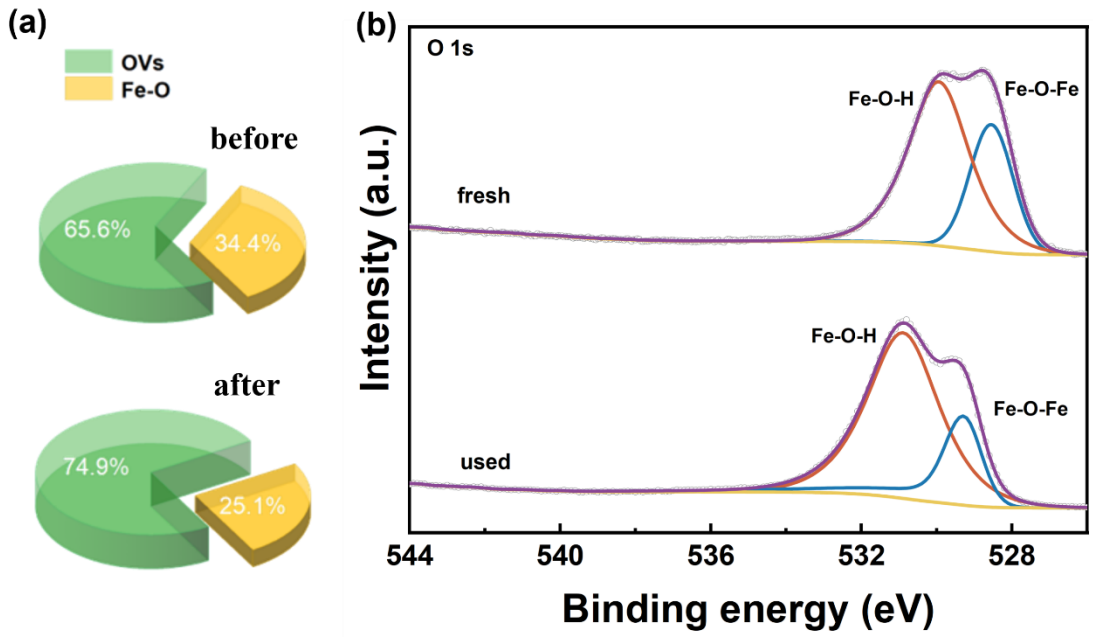

Fig. S15 (a) Changes in the O valence state composition and (b) O 1s XPS spectra of a-FeOOH-Cu^0 before and after the reaction.

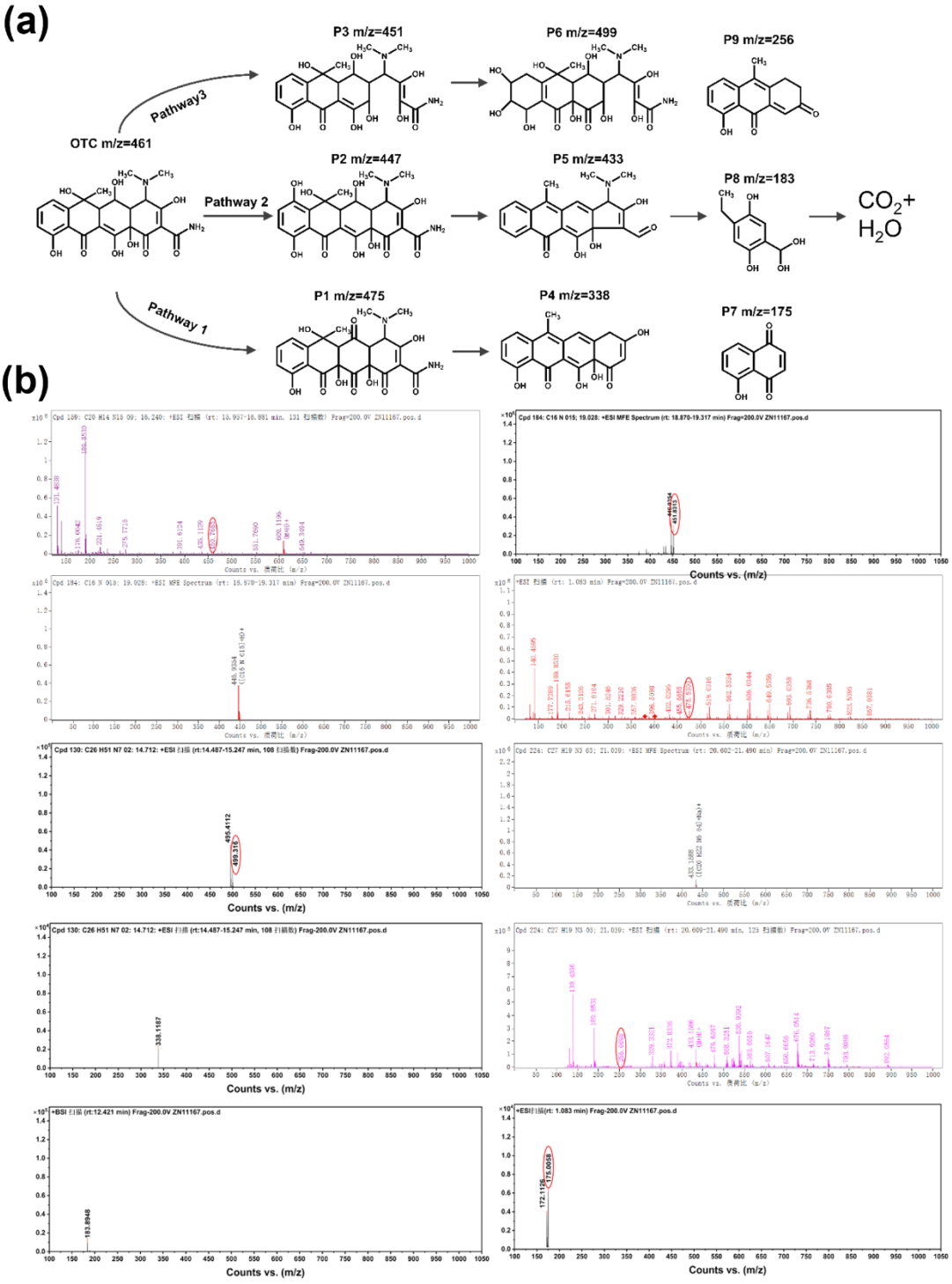

Fig. S16 (a) The degradation pathway of OTC and (b) UPLC-MS analysis of its intermediates in the reaction with a-FeOOH-Cu^0.

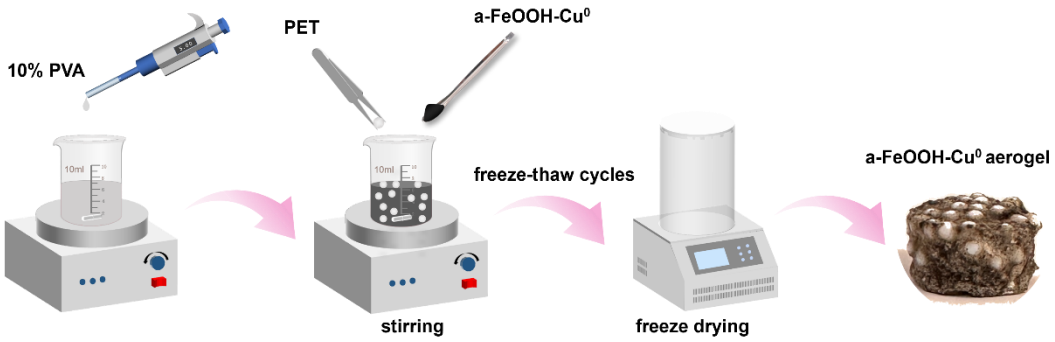

Fig. S17 The preparation of a-FeOOH-Cu^0 aerogel.

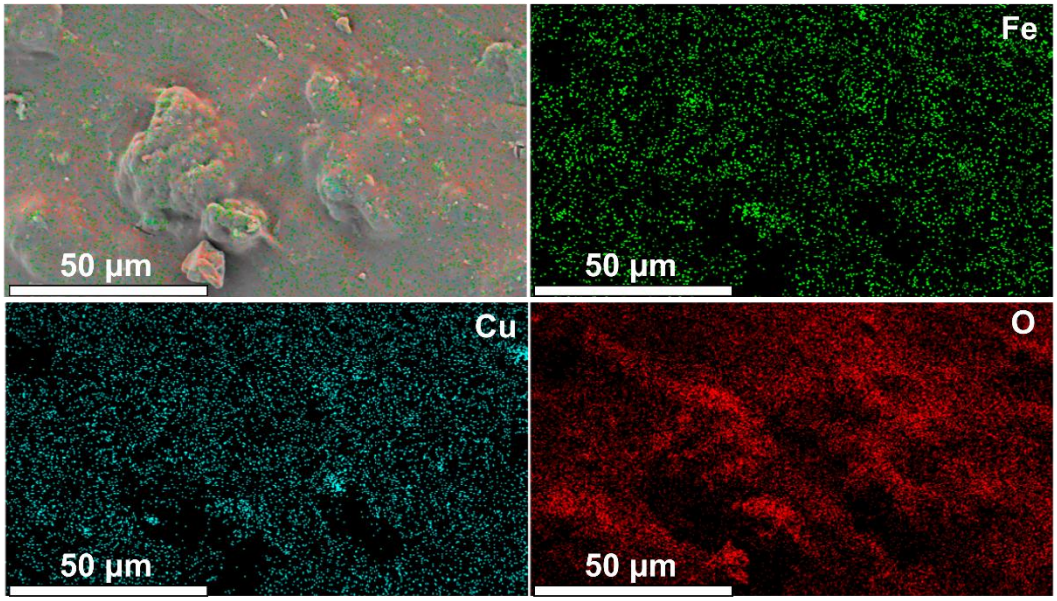

Fig. S18 Energy-dispersive X-ray elemental mapping of a-FeOOH-Cu^0 aerogel.

References

Blöchl P E (1994). Projector augmented-wave method. Physical Review B, 50(24): 17953-17979

Di X, Zeng X, Tang T, Liu D, Shi Y, Wang W, Liu Z, Jin L, Ji X, Shao X (2024). Non-radical activation of peroxymonosulfate by modified activated carbon for efficient degradation of oxytetracycline: Mechanisms and applications. Separation and Purification Technology, 349: 127877

Grimme S, Antony J, Ehrlich S, Krieg H (2010). A consistent and accurate ab initio parametrization of density functional dispersion correction (DFT-D) for the 94 elements H-Pu. The Journal of Chemical Physics, 132(15): 154104

Guo H, Niu C-G, Feng C-Y, Liang C, Zhang L, Wen X-J, Yang Y, Liu H-Y, Li L, Lin L-S (2020). Steering exciton dissociation and charge migration in green synthetic oxygen-substituted ultrathin porous graphitic carbon nitride for boosted photocatalytic reactive oxygen species generation. Chemical Engineering Journal, 385: 123919

Guo Y, Peng Q, Huang Y, Yan S, Luo Y, Xuan K, Hu H, Jiang H, Wang G, Zhao S, Guo Y (2025). In-situ S-doped mesoporous carbon as metal-free catalyst for efficient degradation of oxytetracycline with peroxydisulfate: Performance and mechanism. Separation and Purification Technology, 359: 130763

Hong P, Wu Z, Yang D, Zhang K, He J, Li Y, Xie C, Yang W, Yang Y, Kong L, Liu J (2021). Efficient generation of singlet oxygen ($^1O_2$) by hollow amorphous Co/C composites for selective degradation of oxytetracycline via Fenton-like process.

Chemical Engineering Journal, 421: 129594

Kresse G, Furthmüller J (1996a). Efficiency of ab-initio total energy calculations for metals and semiconductors using a plane-wave basis set. Computational Materials Science, 6(1): 15-50

Kresse G, Furthmüller J (1996b). Efficient iterative schemes for ab initio total-energy calculations using a plane-wave basis set. Physical Review B, 54(16): 11169-11186

Kresse G, Joubert D (1999). From ultrasoft pseudopotentials to the projector augmented-wave method. Physical Review B, 59(3): 1758-1775

Li N, Li R, Duan X, Yan B, Liu W, Cheng Z, Chen G, Hou L A, Wang S (2021). Correlation of active sites to generated reactive species and degradation routes of organics in peroxymonosulfate activation by Co-Loaded carbon. Environmental Science & Technology, 55(23): 16163-16174

Lu H, Sui M, Yuan B, Wang J, Lv Y (2019). Efficient degradation of nitrobenzene by Cu-Co-Fe-LDH catalyzed peroxymonosulfate to produce hydroxyl radicals. Chemical Engineering Journal, 357: 140-149

Perdew J P, Burke K, Ernzerhof M (1996). Generalized Gradient Approximation Made Simple. Physical Review Letters, 77(18): 3865-3868

Ravel B, Newville M (2005). ATHENA, ARTEMIS, HEPHAESTUS: data analysis for X-ray absorption spectroscopy using IFEFFIT. Journal of Synchrotron Radiation, 12(4): 537-541

Ren Z, Che X, Wang Q, Zhang F, Han J, Zhou C, Liang L, Zhu J, Li Z, Li G, Zhan H,

Wang P (2025). RuO_2/MnOOH heterojunctions promotes the formation of high-valent metal-oxo species for ultrafast removal of organic pollutants. Applied Catalysis B: Environment and Energy, 371: 125176

Shi J, Zhao T, Yang T, Pu K, Shi J, Zhou A, Li H, Wang S, Xue J (2024). Z-scheme heterojunction photocatalyst formed by MOF-derived C-TiO_2 and Bi_2WO_6 for enhancing degradation of oxytetracycline: Mechanistic insights and toxicity evaluation in the presence of a single active species. Journal of Colloid and Interface Science, 665: 41-59

Xi Y, Guo X, Han W, Yan H, Zha F, Tang X, Tian H, Zuo Z (2025). BiOBr/FeMoO4 composite achieves oxygen vacancy concentration adjustment to promote persulfate activation degradation of organic pollutants in saline water. Journal of Colloid and Interface Science, 678: 1073-1087

Xie L, Lu X, Huang W, Jiang G, Liu Y, Fan X (2025). Local polarization electric field promoted the active sites formation on the piezo-photocatalytic $BaCaBO_3F$ containing OVs and N doping to effectively degradation of oxytetracycline in water. Separation and Purification Technology, 361: 131637

Yang C, Zhong H, Deng J, Li M, Tang C, Hu X, Zhu M (2025). Z-scheme γ-Fe2O3/g-C3N4 in Photo-Fenton reaction for oxytetracycline degradation: Mechanism study and DFT calculation. Separation and Purification Technology, 354: 129185

Zhang J, Yang X, Deng M, Bai H, Zhang X, Ren J (2025). Construction of Fe-MOF/ZIF derivative C1M5 for efficient activation of PS-degraded OTC by

adsorption-oxidation synergy: Performance and potential activation mechanism. Separation and Purification Technology, 353: 128595

Zhang S, Zhu P, Duan M, He B, Li X, Xin X (2024a). Preparation of direct Z-scheme heterojunction la-doped Bi_2WO_6/CdS with enhanced visible light absorption and its photocatalytic degradation of antibiotics. Separation and Purification Technology, 338: 126524

Zhang Y, Wang M, Chen D, Li N, Xu Q, Li H, Lu J (2024b). Ternary heterojunction of cross-linked benzene Polymer/Bi_2MoO_6-Graphene oxide catalysts promote efficient adsorption and photocatalytic removal of oxytetracycline. Journal of Colloid and Interface Science, 668: 437-447

Zheng X, Yang Y, Yan L, Song W, Li Y, Li X (2025). Efficient production of singlet oxygen via dioxygen activation on Cu^0 decorated MoS_2 facilitates the elimination of oxytetracycline. Journal of Colloid and Interface Science, 679: 656-669